ESCUELA DE CONSTRUCCIÓN CIVIL
FACULTAD DE INGENIERÍA
Revista de la Construcción
Journal of Construction

Research Article

Optimization of fiber-reinforced deep cement-fly ash mixing column materials

Arda Burak Ekmen[1], **Halil Murat Algin**[2]

[1] Department of Civil Engineering, Harran University, Şanlıurfa (Türkiye); ardaburakekmen@harran.edu.tr
[2] Department of Civil Engineering, Harran University, Şanlıurfa (Türkiye); hmalgin@harran.edu.tr
*Correspondence: ardaburakekmen@harran.edu.tr

Received: 19.05.2023; **Accepted:** 22.12.2023; **Published:** 29.12.2023

Citation: Ekmen, A.B., Algin, H.M. (2023). Optimization of fiber-reinforced deep cement-fly ash mixing column materials. Revista de la Construcción. Journal of Construction, 22(3), 722-743. https://doi.org/10.7764/RDLC.22.3.722.

Abstract: The flexural and compressive strength requirements of deep cement mixing (DCM) columns subjected to lateral loading have brought forth the demand to specify how the incorporation of fiber and fly ash improves these properties and the mixture quality, including the construction design characteristics of segregation and swelling. The paper addresses this issue considering the experimental results from the extensive parametric study in which various lengths and content of carbon fiber (4, 6, and 12 mm lengths and 0.1, 0.4, 0.8% by volume of the mixture) are incorporated into the cement-based mixtures with and without the optimized fly ash content. Along the strength parameters, the effects of mixture quality responses on the performance of DCM columns are also investigated. The segregation results of the fresh mixtures, unconfined compression strength (UCS), flexural strength, and swelling values from the 28-day cured specimens are presented. The novel version of the Goal Attainment Method is used for the optimizations, in which the procedures of high-order regression equations and the multi-objective desirability contents are included to obtain more accurate optimization results in terms of the controlling parameters of segregation, swelling, UCS, and flexural strength. The setting time and workability results from the mixtures having the optimized parameters are also presented to demonstrate the fluidity of the optimized mixtures. The addition of carbon fiber led to significant improvements in the segregation and swelling ratios, with gains of up to 35%. Moreover, the three-point flexural strength and unconfined compressive strength were enhanced by 278% and 54%, respectively. The paper specifically reveals that the incorporation of carbon fiber significantly improves the mixture quality characteristics of segregation and swelling as well as the parameters of flexural strength and UCS.

Keywords: Deep cement mixing (DCM), carbon fiber, fly ash, optimization, segregation.

1. Introduction

The deep mixing method, which is one of the most preferred soil improvement techniques, is typically implemented by mechanical dry mixing, wet mixing, or injection (Porbaha 1998; Kamon 1996). DCM columns are widely used to improve the engineering properties of soft soils, effectively reduce the settlement of large-diameter embankments, and provide more economical solutions as an alternative to the piles (Lai et al., 2006; Bergado et al., 1999). DCM columns are also utilized for soft soils where the pile installation is inappropriate. Recent literature includes studies on deep soil mixing stabilization (Dehghanbanadaki et al. 2023). Dehghanbanadaki et al. (2023) conducted a literature review based on small-scale 1 g physical modeling tests of peat stabilized by deep soil mixing. The impact of various binders at varying concentrations on treated peat's compressibility and shear strength characteristics were emphasized in Dehghanbanadaki et al.'s (2023) study. In deep mixing applications, the bonds are formed between the soil particles mixed with the binders such as cement. This enhances the soil's

mechanical properties and prevents geotechnical problems such as liquefaction, excessive settlement, and low bearing capacity (Boehm, 2004; Lorenzo and Bergado, 2006; Shen et al., 2013; Mohammadinia et al., 2019). The bending moments due to lateral loading may cause various mechanical problems in DCM columns having inadequate flexural strength (Sukontasukkul and Jamsawang 2012). For instance, large displacements may occur horizontally due to an embankment on the soil (Wu et al. 2005). In these conditions, an improvement in the flexural strength of DCM columns is required (Sukontasukkul and Jamsawang 2012). Various fiber reinforcements can be used in DCM columns to avoid flexural failures. For instance, in the study of Sukontasukkul and Jamsawang (2012), steel and polypropylene fibers were used to increase the bending performance of DCM columns. Elkhebu et al. (2020) stated that lateral displacements under seismic loadings are likely to occur in the cement-stabilized columns under heavy embankments. This may cause the stabilized columns to collapse due to the bending moments. Elkhebu et al. (2020) investigated the effect of constant fly ash content and the use of polypropylene fiber in the range of 0.5%, 0.75%, 1%, and 1.25% to overcome this failure. Numerous researchers (Duan and Zhang, 2019; Tran et al., 2018; Chen, 2016; Danso et al. 2015; Zhang et al. 2015; Sharma et al. 2015; Mature 2013) argue that fiber reinforcements allow for improving the parameters of strength and deformation while reducing the amount of cement used.

Chen (2016) reported the influence of basalt fiber on the flexural strength of soil stabilized by cement and presented that the maximum flexural strength can be achieved by adding the optimum basalt fiber content to the mixture. The fiber content range of 0.25%–0.5% by weight of dry soil is suggested by Tran et al. (2018) after investigating the effect of waste corn fiber on the strength of cement-stabilized soil. Duan and Zhang (2019) reported the effects of polypropylene fiber (used in the range of 0.1-0.5% by weight of dry soil) and the incorporation of fly ash (used in the range of 0-12% by weight of dry soil) on the flexural strength, UCS, microstructure of cement stabilized soil, deformation properties, and fracture mode of the stabilized soil. Duan and Zhang (2019) stated that for the cement-stabilized soil the unconfined compressive and flexural strength values tend to increase initially and then decrease with the increasing contents of polypropylene fiber and fly ash. Wang et al. (2020) reported that the incorporation of basalt fiber increases the ductility and improves the brittleness of the cemented kaolinite. Anggraini et al. (2017) concluded that the incorporation of coconut fiber into tropical sea clay improves the bending behavior. Gao et al. (2017) examined the effect of the incorporation of carbon fiber on the UCS values of clays and investigated the interaction between soil and fiber using scanning electron microscopy (SEM). It is concluded that the incorporation of carbon fiber increases the UCS values of the soil up to a certain optimum point. Chen et al. (2018) investigated the mechanical behavior of multi-layered Graphene Oxide carbon fiber-reinforced cement composites. It was concluded that the addition of carbon fiber improves the UCS values by approximately 24% and its tensile strength in bending by about 138%. Carbon fiber's low cost and excellent strength have made it the preferred material in numerous research studies.

Cement mortar is produced with high water content during the standard construction phases of deep mixing to facilitate easy pumping and workability without considering the soil layer's natural water content, which can be extremely variable. It is crucial to ensure that the soil and binder mixture has enough water content to achieve the desired ultimate strength obtained from the DCM material (Ekmen et al., 2020). In addition, the water content in the soil layers can also be used to alter the mortar's fluidity, controlling the equipment mobility rate (Croce et al., 2014; Flora et al., 2013). Although it leads to a decrease in the strength and stiffness values, it is generally considered that the amount of water needed in the mixture is double what is required for hydration in order to enable simple pumping. Additionally, it is emphasized that the fly ash additive decreases water requirements by about 10% in an equivalent workability range (Mohammadinia et al.2019; Golder Associates 2013). The use of fly ash provides a sustainable solution to obtain higher strength due to a low calcium supply (Mohammadinia et al.2018 and 2019). An additional advantage of adding fly ash to the mixture is extending the mixture's setting time, which is particularly beneficial in cases of reinforcement is needed (Mohammadinia et al., 2019). Depending on the strength requirements, the binder generally used as Portland cement varies between about 4-20% of the dry weight of the soil in loose form, and this range may vary depending on the field conditions (Porbaha 1998; Porbaha et al. 2000). The incorporation of fly ash induces a reduction in cement consumption, the extension of setting time, and a decrease in water content. Soil improvement using cement and the complimentary binder, particularly fly ash, is a popular research area (e.g., Kafodya and Okonta 2018, Wang et al. 2019). Previous studies (e.g., Broms 1986; Watabe et al. 2000; Yin 2001) based on cemented clay have considered curing time and cement content as the main factors in their parametric research. The natural soil's water content is also a crucial factor affecting the strength of cement-stabilized soil, as investigated by some earlier research (e.g., Miura et al. 2001; Lorenzo and Bergado 2004, 2006). In the presenting study, the use of medium-density clayey, silty sand with the addition of

class F fly ash and carbon fiber reinforcement is considered in terms of the fixed water and cement content previously determined according to the target control strength by Ekmen et al. (2020). The class F fly ash was taken from the thermal power plant in Çatalağzı, Zonguldak (Turkiye), for this investigation. Fly ash is identified by the USEPA (2014) as a non-hazardous waste material and can be used instead of cement in DCM applications.

Some researchers have previously investigated surface soils such as heavily compacted silty clay, loose sand, and silty formations (e.g., Mohammadinia et al. 2019; Lorenzo and Bergado 2006; Boehm 2004; Shen et al. 2013; Porbaha 1998; Porbaha et al. 2000; Terashi 2005). However, there are limited studies that consider clayey, silty sands, which are the soil types rarely encountered in fields of Asia and Europe. Accordingly, medium-density clayey, silty sand is utilized as the soil type in this research to examine the impact of soil improvement induced by the fiber-reinforced deep mixing with and without fly ash incorporation.

It is expected that the stiffness and strength parameters will vary regionally in DCM columns as they are created by mechanical mixing (Liu et al. 2015 and 2019). US Federal Highway Administration (Bruce et al. 2013) suggests that for 28 and 56 days of cured deep mixing specimens, the minimum UCS design values should be considered between 0.7 to 2.1 MPa. Other worldwide design values are similar, ranging about 1 MPa. For instance, specific procedures in Japan prefer 0.5 MPa strength for dry methods, and 1 MPa for wet operations, and this value increases to 1 MPa when lateral force is applied (Terashi 2005). FHWA further notes that the project strength is 1 MPa for soil improvement and 4 MPa for works requiring liquefaction reduction. Research in Thailand (Lorenzo and Bergado 2006) has also utilized this design strength value. Accordingly, the UCS ($qu_{(28)}$) values of the control mixtures in this study were determined as 1 MPa for a 28-day curing period. A series of experiments conducted by Ekmen et al. (2020) were considered to determine the ratios of two different cement-based control mixtures that provide the target UCS, with and without fly ash addition. According to the results of the study by Ekmen et al. (2020), the water content (S_w) for the mixture containing fly ash was determined as 44.55% by weight of dry soil, the cement content (A_w) as 5% by weight of dry soil, and the F class fly ash (FA_w) content as an additional 10% by weight of cement. For the mixture without fly ash, the water content was calculated as 40% by dry soil weight and the cement content as 5.3% by dry soil weight.

Fly ash's contribution to workability, setting time, and evaluation as waste have led to the creation of an alternative control mixture with fly ash that offers the same strength in an environmentally friendly manner. In the presenting study, which is different from the study of Ekmen et al. (2020) carbon fiber was added to these two control mixtures using various fiber lengths (F_L) (i.e., 4 mm, 6 mm, and 12 mm) and the contents by volume (F_C) (i.e., 0.1%, 0.4%, and 0.8%). The main DCM mixture quality characteristics of segregation (on fresh mixtures) and swelling (after a 28-day curing period) have been determined, and the values of UCS and three-point flexural strength (after a 28-day curing period) were identified for all of the specified variations, and the effects of fiber incorporations for the mixtures with and without fly ash were investigated. The optimization analyses were carried out according to the target sets for segregation, swelling, three-point flexural, and UCS ($qu_{(28)}$). Therefore, the results obtained from the presented experimental studies and the optimization analyses indicate some practical suggestions for the optimum design of carbon fiber-reinforced deep mixing applications. The authors further developed and used the Goal Attainment optimization method (GAM) to ensure that the multi-objective desirability scope and well-ordered regression models are incorporated in the optimum target values among the factors considered. Consequently, this process contributed further to a new practical insight into fiber-reinforced DCM optimization.

2. Materials and methods

2.1. *Material*

Carbon fiber is used in this study as a reinforcement to increase the flexural strength and other mechanical properties of DCM columns. The medium-density clayey, silty sand is used as the primary material for the DCM columns, and it is obtained from an excavation in the Şairnabi Campus of Harran University, as in the previous study conducted by Ekmen (2020). The sampling was conducted between 4 and 5 meters deep. Table 1 provides the physical characteristics of sand used in the presenting study. The soil used in this study was dried at a room temperature of approximately 25 °C, and the soil passing through the No. 4 sieve (i.e., the diameter of 4.75 mm according to the US standard) was stored in closed bags until used in

the experiments. The chemical composition of the natural soil, the fly ash and the cement (CEM IV / BP-32.5N) obtained from XRF (X-ray fluorescence) analysis is given in Figure 2.

Table 1. The physical characteristics of sand used.

Properties	Values
G_s	2.69
γ_n	18.2–19.3 kN/m^3
γ_{dry}	16–16.9 kN/m^3
D_r	0.64
D_{10}	0.01
D_{30}	0.06
D_{50}	0.20
D_{60}	0.31
C_u	1.55
C_c	0.06
e_0	0.65
e_{max}	0.8
e_{min}	0.56
w_n	13.5–13.9%
liquid limit (LL)	56%
plastic limit (PL)	32%

The particle size distribution of medium-density clayey, silty sand used in this study is shown in Figure 1 (Ekmen et al. 2020).

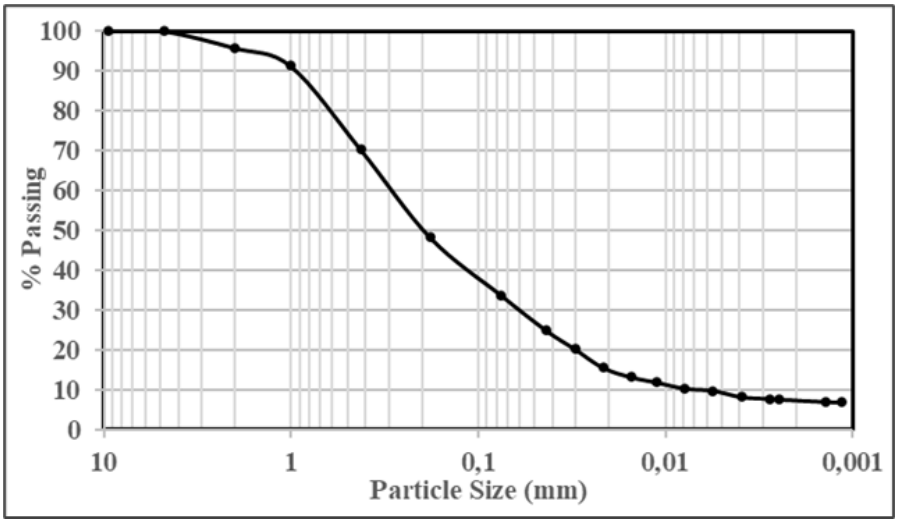

Figure 1. Gradation of medium-density clayey, silty sand (Ekmen et al. 2020).

Class F fly ash utilized in the presented study was obtained from Çatalağzı thermal power plant in Zonguldak (Turkiye) (Gs = 2.0). Figure 3 (d) demonstrates the result of the X-ray diffraction (XRD) examination by Ekmen et al. (2020) on the dried soil specimens passing through the 75 µm (No. 200) sieve. Operations were performed by Ekmen et al. (2020) utilizing a Philips X-ray diffractometer to describe the characterization of the clay mineral with monochromatic radiation and the soil specimen was heated at 60°C for three days. The sample was established in an XRD specimen holder in order to rapidly determine the range below 60%RH. XRD analysis showed the presence and mineralogical properties of montmorillonite clay

as well as other minerals such as gibbsite, quartz, goethite, and jarosite in the relevant soil sample. Figure 3 (a-c) shows the outcomes of XRD analyses on fly ash per se, samples from the mixture produced with cement-fly ash combination, and cement, respectively. CASH and CSH gels, indicative of the hydration reaction in soil stabilized with fly ash and cement, can be seen in the XRD test presented in Figure 3 (b).

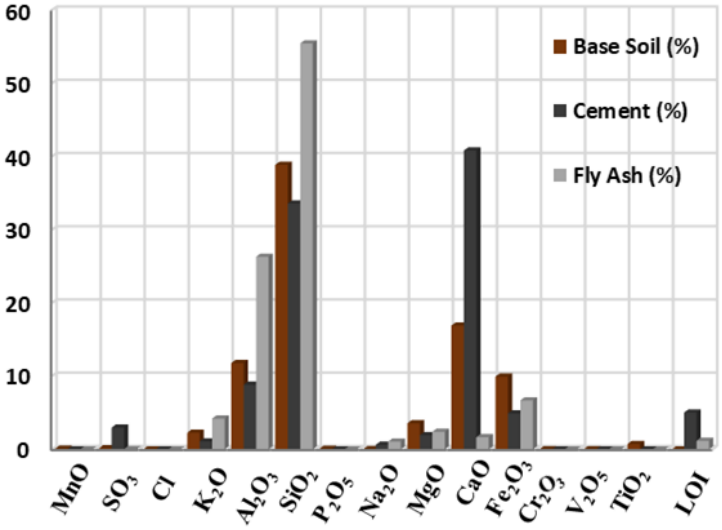

Figure 2. Chemical composition of the base soil, cement, and fly ash.

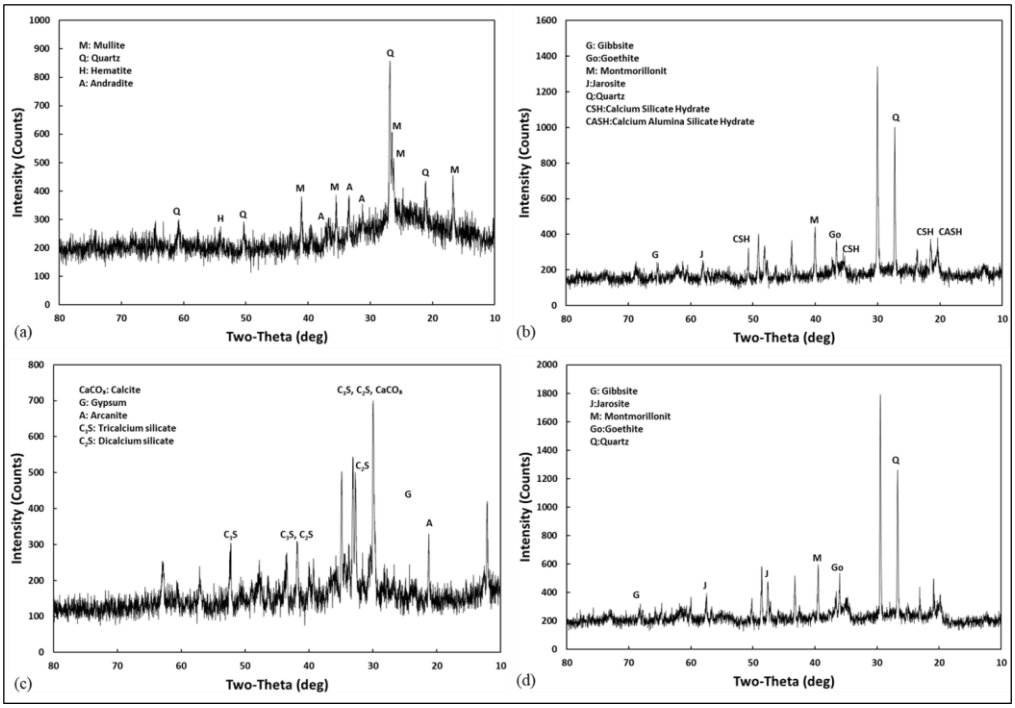

Figure 3. XRD analyzes (a) fly ash, (b) fly ash and cement-improved soil, (c) cement, (d) natural soil (< 75 μm) (Ekmen et al. 2020).

2.2. *Sample preparation and tests*

The mix design ratios were selected for two different cement-based control mixtures providing 1 MPa UCS value ($q_{u(28)}$) with and without fly ash, considering the study of Ekmen et al. (2020). For the mixture containing fly ash, the water content (S_w) was specified as 44.55% by weight of dry soil, the cement content (A_w) was selected as 5% by weight of dry soil, and the Class F fly ash (FA_w) content was determined as 10% by weight of cement as an addition to the binder. For the mixture without fly ash, the water content (S_w) was chosen as 40% by weight of dry soil, and the cement content (A_w) was determined as 5.3% by weight of dry soil. 18 different mixtures were produced by adding carbon fiber for all variations using the fiber lengths of 4, 6, and 12 mm (F_L) and incorporating with the contents of 0.1, 0.4, 0.8% by volume of the mixture (F_C). Since the specimen preparation procedure is one of the most critical processes affecting the ultimate sample strength (Chen et al. 2011; Bruce et al. 2013), the mixing technique described in the FHWA guidance (Bruce et al. 2013) was used to prepare the samples. In order to adjust the consistency of the mixture in accordance with the targeted water content, a fiber-added mortar with 30% water content without soil samples was prepared.

The mortar was mixed with a portable mechanical mixer equipped with a mixing apparatus for 3 minutes. In another mixer which was used to attain homogeneous mixtures, the remaining amount of water was gradually admixed to the soil sample to reach the target water content. Then, these two mixtures were combined and mixed in a portable mixer for 10 minutes until a homogeneous mixture mortar was obtained. The combinations were subjected to a segregation test while remaining fresh in compliance with ASTM C1610/C1610M-17 standards (Figure 4-d). The three-part segregation mold consisting of lower, middle, and upper parts with a diameter of 200 mm and a height of 660 mm was filled with fresh mixture within 2 minutes as specified in the standard. After the mold was filled, a shear bar was used to align the mix surface with the top of the mold. After the mixture was left in the mold for 15 minutes, the upper part of the mold was held tightly, and the contact system was removed. The remaining processes were focused on finishing in the allowed 20 minutes per the established standard. The mixture at the top and bottom of the mold was removed using a horizontal rotational motion and taken into a separate container. Similarly, the mix in the middle part was released and discarded for use. The static segregation ratio was determined according to the remaining coarse aggregate masses by separating the mixtures taken from the lower and upper parts of the mold.

For the unconfined compression test, the mixtures were transferred to PVC specimen molds with inner diameters of 100 mm and heights of 200 mm (Figure 4-c). After one day, the samples were removed from the molds and airtightly wrapped by applying a slim silicone layer to the plastic curing packages so that they could retain the 97% water content at 25°C ambient temperature. Air conditioners were used in the laboratory to keep the room temperature constant during the curing process. Three pushers were used to transport highly workable non-liquid substances into sample tubes. Apparatus removal operations were carried out by gradually tapping a thin rod on each pusher apparatus to eliminate the air gaps formed and prevent the mixture from having a perforated structure. This process aims to simulate the actual situation of deep mixing column production (Ekmen et al. 2020).

Lorenzo and Bergado (2004, 2006) also suggested this approach. The diameter/height ratio of the UCS test samples was determined to be 0.5 as specified in the FHWA guide (Bruce et al., 2013). In order to get a flat surface, which is essential in the UCS test, leveling was applied by methodically examining the surface with each dice's straight edge. Considering the FHWA guideline (Bruce et al. 2013), samples with a density less than 95% of the density of the weightiest sample were eliminated to prevent the negative impact of air voids, and the remaining samples were selected for the UCS test. The UCS tests were carried out in accordance with the ASTM D2166 standard using a deformation rate of 0.1 mm/s (Figure 4-h). Experiments were carried out behind curing times of 28 days. Three samples were tested, and the test results were averaged for each mixture.

The mixtures to be subjected to the three-point flexural test were transferred to metal molds with the dimensions of 100x100x350 mm (Figure 4-a). The samples were removed from the molds after one day and wrapped airtight by using a slim silicone layer to the plastic curing packages to keep the 97% water content at 25°C ambient temperature as applied to the samples left for the UCS test. The current version of the ASTM C1609 standard (ASTM C1609 / C1609M-19) used by Sukontasukkul and Jamsawang (2012) was applied for the DCM samples to be subjected to the three-point flexural test. Experiments were carried out at 300 mm mount spacing, using a deformation rate of 0.1 mm/s following the relevant standard

after a 28-day curing period (Figure 4-f). Three samples were tested for each admixture, and the test results were averaged. The mixtures to be subjected to the swelling test were transferred to metal molds with a diameter of 50 mm and a height of 20 mm (Figure 4-b). After one day, the samples were removed from the molds and airtightly wrapped by using a slim silicone layer to the plastic curing packages to keep the water content at 97% at 25°C ambient temperature.

Figure 4. Sample preparation and experiments; (a, b, c) prepared samples, (d) segregation test, (e) consolidation test, (f) three-point flexural test, (g) triaxial test, (h) unconfined compression test.

The swelling test was conducted following the ASTM D4546–14 standard. Among the methods in the relevant standard, method B was selected and applied. Three samples of each mixture were evaluated during the experiment using completely automatic consolidation equipment (Figure 4-e), and the outcomes were averaged. As recommended by Lorenzo and Bergado (2004, 2006), the oedometer ring for the natural soil in this investigation was employed directly in the oedometer experiment to avoid dispersion. Specimens with a diameter of 67.5 mm were obtained from the drilling made for the triaxial test to be applied to the natural soil and were directly sealed without exposure to the open air. The specimens were maintained at consistent humidity and heat levels in the laboratory and transferred to a fully automatic three-axis test device without being disturbed. With the initial saturation degree set to 95% for all samples, saturation steps were conducted with a fully automated triaxial tester in accordance with ASTM D 4767-88 standards (Figure 4-g).

3. Experimental results and analysis

3.1. Results of the studied natural soil

The test results obtained from triaxial tests performed on natural soil as isotropically consolidated undrained (CIU) are shown in Table 2. Tests were performed following ASTM D 4767-88. In order to avoid excessive sample consolidation and ensure proper saturation, the typical saturation technique was utilized. The back pressure was calculated to be 630 kPa, and the initial saturation level was 95%. Consolidation was performed by applying 100 kPa pressure (K0) to all samples in an isotropic manner to reflect the field conditions. The results of the CIU experiments in this study agree with previous studies on clayey, silty sands (e.g. Soranzo 1988, Shahin and Cargeeg 2011). Three different cell pressures (i.e., 150, 300, and 450 kPa) were used for these testing. Three tests were performed for each mixture combination, and the average of the tests was designated as specified in the ASTM standard (D4767). The data from the consolidation test for the natural soil are demonstrated in Table 2, along with the UCS of the natural soil (q_u). The pre-consolidation pressure is 80.5 kPa, and the swelling and compression indices are 0.0086 and 0.047, respectively, according to the relevant table.

Table 2. Test results for the natural soil.

Material	Natural soil
q_u (kPa)	152
c' (kPa)	25.37
Φ' (°)	33.4
C_c	0.047
C_s	0.0086
Preconsolidation pressure (kPa)	80.5

3.2. Test results for fiber-reinforced soil

Results from the UCS and the three-point flexural strength tests performed on 28-day cured control mix and fiber-reinforced samples are presented in Figures 5-7. The unconfined stress-strain and three-point flexural stress-deformation curves were obtained for all variations of mixtures with and without fly ash incorporations and for the fiber lengths of 4 mm, 6 mm, and 12 mm (F_L) and for the fiber contents (F_C) of 0.1%, 0.4%, and 0.8% by the mixture volume. The UCS values ($q_{u(28)}$) in Figure 5 (a-b) and the three-point flexural strength values (f_{dmc}) in Figures 6 (a-b) are collected in a single graph, separating the cases with and without fly ash addition in order to compare all variations with each other. Figure 7 (a-d) shows the effect of the variation in carbon fiber reinforcement percentage by volume on the mechanical characteristics of the soil. Figure 5 demonstrates that the unconfined compressive stress-strain curves are significantly influenced by the amount of fiber reinforcement.(F_C) both in the samples with and without fly ash addition.

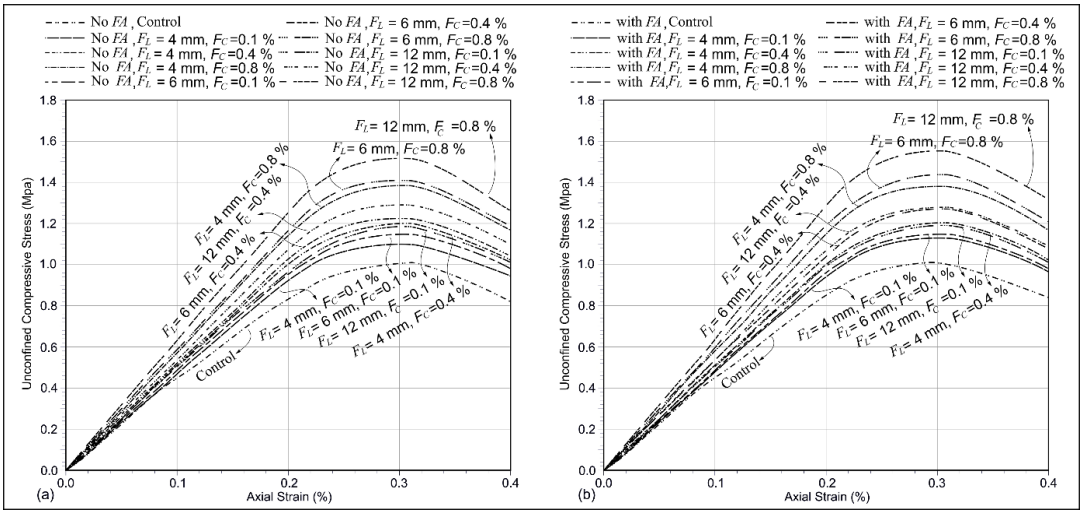

Figure 5. UCS values for all variations ($q_{u(28)}$); (a) variations without fly ash, (b) variations with fly ash.

Increasing the fiber content from 0.1% F_C to 0.8% F_C resulted in an increase of approximately 22%-30% in UCS values ($q_{u(28)}$) and modulus of elasticity ($E_{u(28)}$) for all fiber lengths (F_L) (Fig. 6-a). As can be seen, both samples with and without fly ash incorporation have different effects on the unconfined stress-strain curves in Figure 5. Increasing the fiber length from F_L=4mm to F_L =12mm improves the UCS values by about 5%-13% for all fiber contents (F_C). The combination of 0.8% F_C and F_L = 12mm for samples with and without fly ash incorporation provided the highest UCS value compared to the control mixtures without fiber reinforcement. The UCS values from the fiber-reinforced samples with and without fly ash addition are increased by approximately 54% and 50%, respectively, compared to the control mixtures (A_w=%5, S_w=%44.55, FA_w=%10, F_C=%0 and A_w=%5.3, S_w=%40, F_C=%0), which have 1 MPa UCS value. These results agree with the previous studies in the literature (Chen et al. 2018; Gao et al. 2017) investigating the effect of carbon fiber.

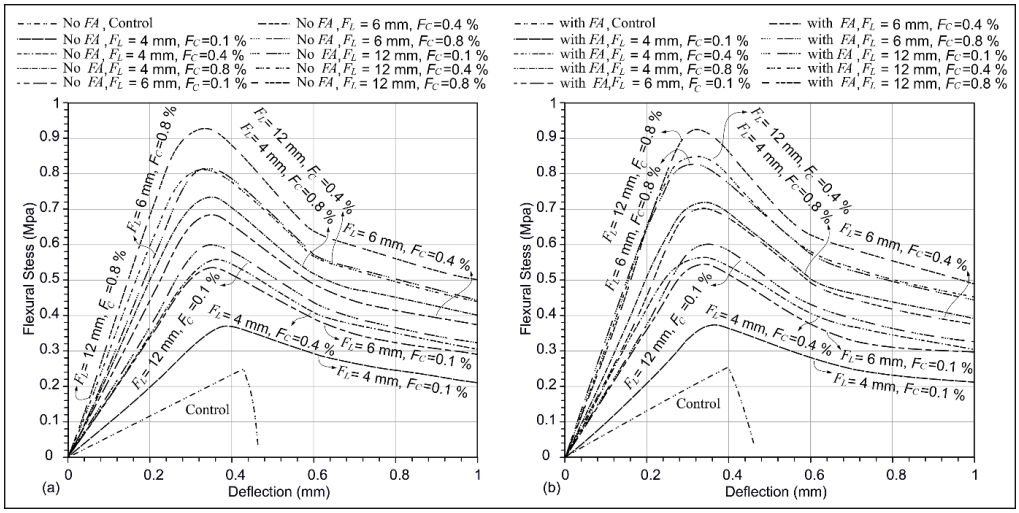

Figure 6. Three-point flexural strength values (f_{dmc}) for all variations; (a) variations without fly ash, (b) variations with fly ash.

It was determined that the UCS value ($q_{u(28)}$) of the samples obtained from fiber-reinforced and fly ash-incorporated mixtures were higher than the samples produced in all fiber lengths (F_L) variations obtained from the equivalent combinations without fly ash incorporations (Figure 7-a). It is seen that the increase in both parameters provides an improvement in terms of UCS values when all fiber lengths (F_L) and contents (F_C) are examined. In addition, the increase in fiber content (F_C) improves the UCS values ($q_{u(28)}$) effectively compared to the increase in fiber length (F_L). The percentage of contribution

calculated using the statistical analysis of variance provided in the presented section titled ‘Statistical Evaluation’ also supports this conclusion.

The three-point flexural stress-deformation curves are significantly affected by the fiber content (F_C), as shown in Figure 6, in both the samples with and without the fly ash incorporation. Increasing the fiber content from 0.1% to 0.8% results in an improvement of approximately 55%-98% in three-point flexural strength ($q_{u(28)}$) for all fiber lengths (Fig. 6-c). The three-point flexural stress-deformation curves in Figure 6 can be demonstrated to be affected by fiber length in both samples with and without fly ash addition. For all fiber contents, increasing the fiber length from 4mm to 12mm enhances the three-point flexural strength by approximately 25%-60%. In comparison to control mixtures without fiber reinforcement, the samples with and without fly ash addition that combined 0.8% F_C and F_L = 12mm had the highest three-point flexural strength. In comparison to the control mixes (A_w=%5, S_w=%44.55, FA_w=%10, F_C=%0 and A_w=%5.3, S_w=%40, F_C=%0), which have three-point flexural strengths (f_{dmc}) of 0.25 and 0.245 MPa, the fiber-reinforced sample with and without fly ash addition had an increase in three-point flexural strength of approximately 267% and 278%, respectively. These results agree well with the study conducted by Chen et al. (2018). The three-point flexural strength of the samples produced in all fiber lengths (F_L) obtained from the equivalent mixtures without fly ash incorporations were determined to be lower than the samples produced in 0.4% fiber content and fly ash addition (Figure 7-c). It was determined that the increase in both parameters provided an improvement in terms of three-point flexural strength when all fiber lengths and fiber contents were examined. It was concluded that the increase in fiber content is a more effective parameter in improving the three-point flexural strength than the increase in fiber length. The percentage of contribution calculated using the statistical analysis of variance provided in the study's section on ‘Statistical Evaluation’ also supports this conclusion.

Figure 7-b illustrates how the fiber content and the fiber length affect the swelling percentage in samples with and without fly ash incorporation. The swelling was determined as 2.1% for the sample obtained from the control mixture without fly ash addition and as 2.02% for the control mix with the incorporation of fly ash. Increase in the fiber content from 0.1% to 0.8% results in a decrease in swelling percentage by approximately 18%-24% for all fiber lengths (Figure 7-b). Figure 7-b shows that for the same F_L values, the percentage of swelling reduces as the F_C values rise. Increase in the fiber length from 4mm to 12mm results in a 6%-9% decrease in the swelling ratio for all fiber contents. The swelling ratio was shown decreasing with an increase in F_L values for the same F_C values (Fig. 6-b).

In comparison to control mixtures without fiber reinforcement, the combination of 0.8% F_C and F_L =12mm for fly ash addition, and samples without fly ash addition provide the lowest swelling ratio. Due to the specific fiber reinforcement, the swelling ratio of the specimens with and without fly ash addition decreases by almost 35% compared to the control mixes (A_w=%5, S_w=%44.55, FA_w=%10, F_C=%0 and A_w=%5.3, S_w=%40, F_C=%0). The samples produced in all fiber lengths, obtained from the equivalent mixtures without fly ash incorporations, show higher swelling ratios than the mixtures with fiber reinforcement and fly ash addition (Figure 7-b). This positive outcome provided by the fly ash incorporation is consistent with the study conducted by Ramadas et al. (2010). When all fiber lengths and contents are examined, it is concluded that the increase in both parameters provides a reduction in the swelling ratios. Additionally, the increase in fiber content is more effective in improving the swelling ratios than the fiber length increment. The contribution was calculated using the statistical analysis of variance provided in the section presented in this paper, as the title of ‘Statistical Evaluation’ also supports this conclusion.

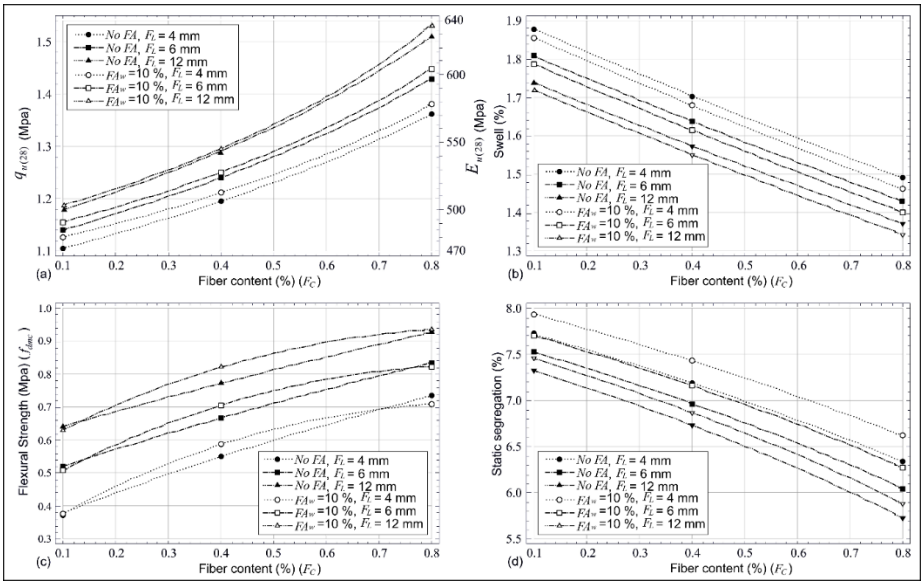

Figure 7. Effects of the carbon fiber content; (a) 28-day UCS values ($q_{u(28)}$) and the elasticity modulus($E_{u(28)}$), (b) swelling ratio, (c) three-point flexural strength values (f_{dmc}), (d) static segregation ratio.

Figure 7-d demonstrates that the segregation ratio is influenced by the amount of fiber and the fiber length both in the samples with and without fly ash addition. The segregation was determined as 8.6% for the sample obtained from the control mixture without fly ash addition and 8.69% for the control mixture with fly ash addition. Increase in the fiber content from 0.1% to 0.8% results in a decrease in the segregation ratio by approximately 16%-23% for all fiber lengths (Figure 7-d). Figure 7-d shows that for the same F_L values, the segregation ratio decreases as F_C values rise. Increase in the fiber length from 4mm to 12mm results in a 5%-13% decrease in the segregation ratio for all fiber contents, and it was determined that the segregation ratio decreases with an increase in $F_L$values for the same F_C values (Fig. 6-d).

The combination of 0.8%F_C and F_L=12mm for fly ash addition, and samples produced without fly ash show the lowest segregation ratio compared to the control mixtures without the incorporation of fiber. The segregation ratio of the samples with and without the fly ash incorporation is decreased by about 34% as a result of the fiber addition compared to the control mixes (A_w=%5, S_w=%44.55, FA_w=%10, F_C=%0 ve A_w=%5.3, S_w=%40, F_C=%0). It was determined that the increase of both parameters specified in the variations of whole fiber length and content led to a decrease in the segregation ratio. The increase in fiber content was indicated to be more beneficial than the increase in fiber length in enhancing the segregation ratio. This result is also confirmed by the statistical analysis of variance used to compute the percentage of contribution, which is presented in the section titled 'Statistical Evaluation'. It was concluded that the carbon fiber addition improves all the investigated parameters, and the most significant effect was on the three-point flexural strength values.

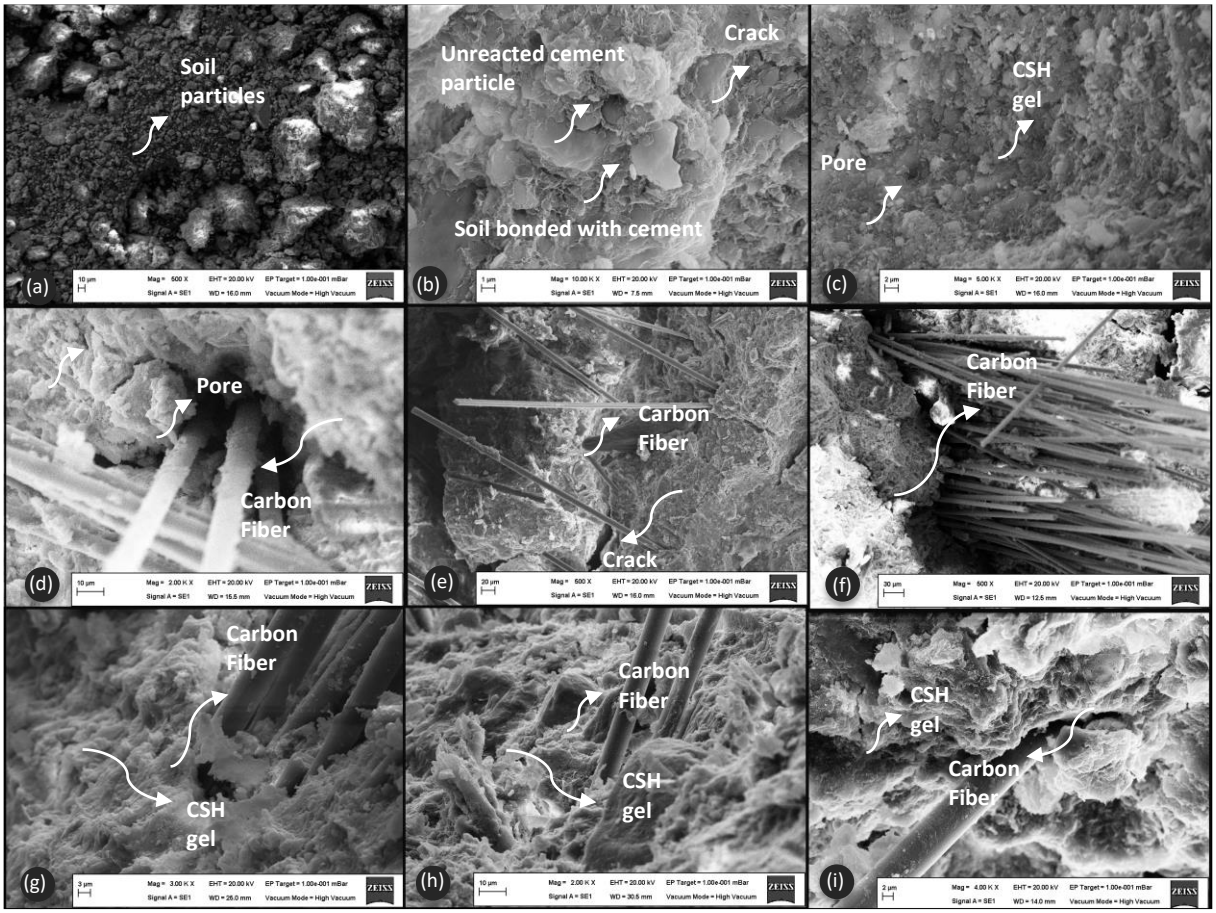

Figure 8. SEM images, (a) natural soil, (b) 28 days cured control sample without fly ash addition, (c) 28 days cured control sample with fly ash addition, (d) carbon fiber reinforced sample without fly ash addition (F_C=%0.1 F_L=4 mm), (e) carbon fiber reinforced sample without fly ash addition (F_C=%0.4 F_L=6 mm), (f) carbon fiber reinforced sample without fly ash addition (F_C=%0.8 F_L=12 mm), (g) carbon fiber reinforced sample with fly ash addition (F_C=%0.8 F_L=4 mm), (h) carbon fiber reinforced sample with fly ash addition (F_C=%0.4 F_L=6 mm), (i) carbon fiber reinforced with fly ash addition sample (F_C=%0.1 F_L=12 mm).

The SEM image of the base soil is shown in Figure 8 (a). Figures 8 (b-c) illustrate the SEM images of the control sample cured for 28 days without and with the fly ash addition, respectively. SEM images of carbon fiber reinforced samples with and without fly ash addition in a range of length and content are shown in Figure 8 (d–i). The SEM illustrations in Figure 8 demonstrate the compounds produced after hydration, the condensation due to stabilization, and the distribution of carbon fibers. The figure also shows the cement particles that have reacted or not reacted, voids in the materials, CSH gels formed during hydration, and soil particles that have reacted with cement. Figures 8 (d-i) show that the soil-cement mixture and carbon fibers are well bonded owing to hydration products and the cement's binding ability. It has also been detected that the distribution of carbon fibers added to the mixture balances the mixture depending on the fiber content (Figures 8d-8i). Due to its pozzolanic impact, fly ash increases the hydration products in Figure 8 (g–i). Therefore, CSH gels provide a denser structure by allowing them to fill more voids.

3.3. Optimization based on the goal attainment method

The goal attainment method (GAM) was developed by Gembicki (1974). Engineering design goals can be achieved using the GAM. The GAM function is incorporated in MATLAB (2017) and offers numerical solutions to the problems. With this approach, problems are attempted to be resolved by concentrating on the targets. The problem is defined with a single solution set considering the weight coefficients and goal values in this method. A weighting coefficient vector controls the degree to which design goals are achieved. This optimization method is formulated as follows (Ekmen et al. 2020):

$$\min_{f \in R, p \in U} f \quad (1)$$

$$\varphi_k(p) - w_k f \leq \varphi_k^*, k = 1,2,\ldots,n, \quad (2)$$

In Equations 1 and 2, *U* denotes the universal set for probable design parameters of *p*, k denotes the *i*th target, *f*, represents the target function, ϕ_k , indicates the target, ϕ_k^* , means the design target, and w_k indicates the weight coefficient (Ekmen et al. 2020). This method provides a convenient solution to engineering problems with the advantage of nonlinear programming capability (Liu et al. 2003). The existing literature provides several instances where the relevant optimization techniques have been improved and implemented successfully (Ekmen, 2023; Avci and Ekmen, 2023; Ekmen and Avci, 2023).

Using nonlinear programming with GAM, additional inequalities with physical restrictions can also be added to the problem. This feature allows the practitioner to explore possible solutions to the problem (Ekmen et al. 2020). Therefore, nonlinear programming facilitates designs by providing the practitioner with information about conflicting design requirements. Although the primary function of GAM is incorporated in MATLAB (2017), no multiple desirability features exists among the main functions provided for GAM. In addition to the existing capabilities of GAM, the specification of a desirability factor for the overall design and the ability to generate desirability range graphs were included in the optimization algorithm by Ekmen (2020). As shown in Equation 3, in this method, the desirability (D) value is obtained by calculating the geometric mean of the desirability values (d_k) acquired separately for all outputs, as follows (e.g., Pradeep 2008, Myers et al. 2009, Algin 2016). The Response Surface Method (RSM) was considered in this methodology.

$$D = (d_1 \times d_2 \times d_3 \times \ldots \times d_n)^{1/k}, \quad (3)$$

The desirability (D) value obtained in the developed method changes in the range of $0 \leq D \leq 1$. A value of "1" indicates that all desired targets have been fully achieved, and if the D value is "0", it indicates that the desired state has been exceeded. This GAM-based interface can incorporate a user-defined model representing the experimental data into the solution of the optimization problem. Within the scope of this study, various graphical solutions were obtained with the relevant coding used in optimization analysis. Since the optimization method used has the ability to import functions, it allows higher desirability values to be achieved.

3.3.1. Statistical evaluation

A method known as GLM-ANOVA reveals the statistical significance of the effect of various factors on dependent variables. The effects of the factors considered in this study (F_C and F_L as the independent variables) on the dependent variables (The values of UCS, three-point flexural strength, swelling, and segregation) were evaluated utilizing the general linear model analysis of variance (GLM-ANOVA). Table 3 displays the ANOVA outcomes for the parameters of UCS, three-point flexural strength, swelling, and segregation based on the data shown in Figure 7. The analyses were performed at a 95% confidence level for each dependent variable to demonstrate the impact of the factors on the results (Table 3). The parameters in the analysis of variance in this study are categorical.

Table 3. ANOVA results.

Dependent variables	Independent variables	Statistical Parameters					Significance	Contribution (PC_x) (%)
		Degrees of freedom (*df*)	Sum of square (SS_x)	Mean square (MS_x)	F	P-Value		
$q_{u(28)}$	F_L	2	0.0168	0.0084	23.92	<0.006	Yes	11.04
	F_C	2	0.1338	0.0669	190.78	<0.001	Yes	88.04
	Error	4	0.0014	0.0004				0.92
$q_{u(28)}^{FA}$	F_L	2	0.0172	0.0086	6.99	<0.05	Yes	10.56
	F_C	2	0.1413	0.0706	57.27	<0.002	Yes	86.42
	Error	4	0.0049	0.0012				3.02
f_{dmc}	F_L	2	0.076	0.038	62.56	<0.001	Yes	32.02
	F_C	2	0.1589	0.0795	130.83	<0.001	Yes	66.96
	Error	4	0.0024	0.0006				1.02
f_{dmc}^{FA}	F_L	2	0.0862	0.0431	54.96	<0.034	Yes	35.37
	F_C	2	0.1544	0.0772	98.44	<0.002	Yes	63.35
	Error	4	0.0031	0.0008				1.28
$Segregation$	F_L	2	0.3713	0.1856	15.01	<0.02	Yes	9.65
	F_C	2	3.4251	1.7125	138.48	<0.001	Yes	89.06
	Error	4	0.0495	0.0124				1.29
$Segregation^{FA}$	F_L	2	0.5501	0.275	21.35	<0.008	Yes	14.46
	F_C	2	3.2018	1.6009	124.26	<0.001	Yes	84.18
	Error	4	0.0515	0.0129				1.36
$Swelling$	F_L	2	0.0266	0.0133	14.25	<0.02	Yes	10.88
	F_C	2	0.2141	0.107	114.68	<0.001	Yes	87.59
	Error	4	0.0037	0.0009				1.53
$Swelling^{FA}$	F_L	2	0.0242	0.0121	23.63	<0.007	Yes	9.64
	F_C	2	0.2244	0.1122	219.48	<0.001	Yes	89.54
	Error	4	0.002	0.0005				0.82

(*) "FA" superscript denotes that the relevant samples contain fly ash.

Since all the p-values in Table 3 are less than 0.05, it can be concluded that every factor has a statistically significant impact on the results. Regression analysis was utilized in order to develop the estimation models for the dependent parameters. The percentage contribution (PC_x) of each independent variable was determined using the Taguchi technique (e.g., Ben-Gal 2005, Algin 2016 and Algin 2018, Ekmen et al. 2020). Table 3 indicates that all factors contributed 100% of the total percentage, including the error term. Higher numbers indicate a more significant impact of the independent variables on the results. The independent variable F_C is the essential factor for all dependent variables, as seen in Table 3.

The statistical analyses were carried out using MATLAB (2017), and a total of eight models were considered for each output (Table 3). All input parameters used in the calculation iterations were considered and incorporated into the research

models. The R^2 values of the models determined by regression analyses fell within the range of 0.96-0.99, which indicates that the actual data and expected results are well correlated.

3.3.2. Results of optimization analysis

The dependent and independent variables for the multi-objective optimization analyses utilizing GAM are shown in Table 4. In the presented optimization, equal weights are used for all outputs, and identical priorities are defined. The composite singular desirability value is defined in Equation 3. The optimization goals and the parameter ranges are given in Table 4. The upper and lower limits in Table 4 were determined by considering the limits in the experimental data.

Table 4. Variable definitions for the multi-objective optimization process.

	Parameters	Goal	Lower limit	Upper limit
Factors	$F_L\ (mm)$	In range	4	12
	$F_C\ (\%)$	Minimize	0.1	0.8
Outputs	$q_{u(28)}(MPa)$	In range	1.1	1.52
	$q_{u(28)}^{FA}(MPa)$	In range	1.13	1.56
	$f_{dmc}(MPa)$	Maximize	0.37	0.93
	$f_{dmc}^{FA}(MPa)$	Maximize	0.37	0.93
	$Segregation\ (\%)$	Minimize	5.65	7.68
	$Segregation^{FA}(\%)$	Minimize	5.81	7.95
	$Swelling\ (\%)$	Minimize	1.36	1.9
	$Swelling^{FA}(\%)$	Minimize	1.33	1.86

(*) "FA" superscript denotes that the relevant samples contain fly ash.

Since fiber utilization affects the general cost, the fiber content is minimized in the optimization. The most desirable results from the optimization analyses are presented in Table 5. Figure 11 demonstrates the composite desirability variation acquired from these optimization analyses, including the desirability graphs with the solutions given in Table 5. The optimal solutions of Table 5 fall between the upper and lower bounds presented in the ranges of Table 4. The optimization results in Table 5 have the highest desirability values of about 0.82. These values indicate that the targets presented in Table 4 were achieved sufficiently. It can also be seen in Figures 9-11 that the results obtained as a result of the optimization corresponding to the values of the independent variables are in good agreement with the experimental values.

Table 5. Results of the optimization analysis and workability-setting time experiments.

Outputs		$F_L\ (mm)$	F_C (%)	Desirability	Setting time (min) start–end	LL (%)	PL (%)	PI
$q_{u(28)}(MPa)$	1.3	12	0.4	0.78	149–231	48.2	40.4	7.8
$f_{dmc}(MPa)$	0.8							
$Segregation$ (%)	6.73							
$Swelling$ (%)	1.57							
$q_{u(28)}^{FA}(MPa)$	1.3	12	0.4	0.82	188–273	47.3	40.5	6.8
$f_{dmc}^{FA}(MPa)$	0.83							
$Segregation^{FA}(\%)$	6.78							
$Swelling^{FA}(\%)$	1.55							

(*) "FA" superscript denotes that the relevant samples contain fly ash.

The desirability value of the mixture with the fly ash addition is higher than that of the mixture without the addition of fly ash, and this demonstrates that the desired solution is more attainable in the mixture with fly ash incorporation. Figure 9 (a-d) presents 3D regression graphs showing the effect of factors (F_C and F_L) on the dependent parameters for the samples without fly ash addition.

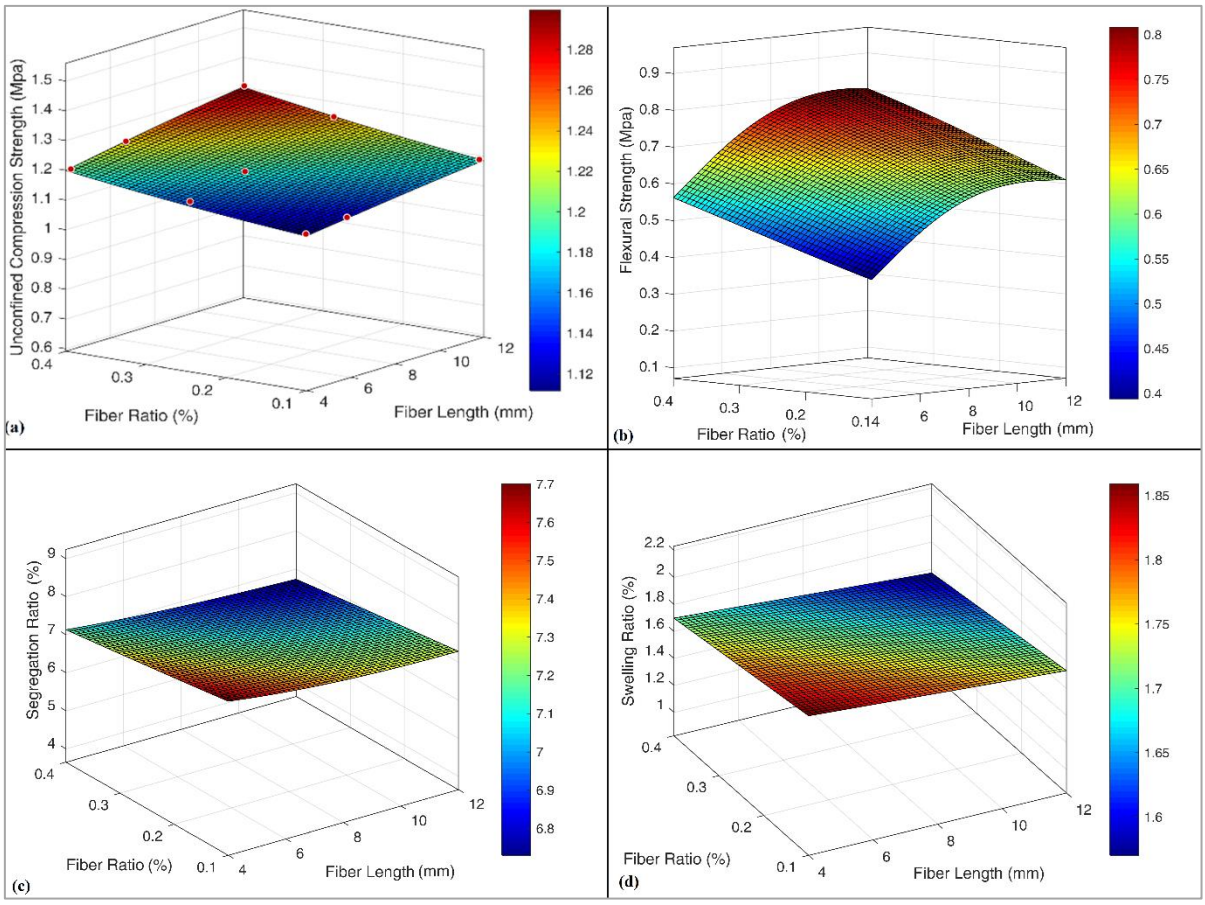

Figure 9. 3D regression plots showing the effect of factors (F_C and F_L) on the responses from the mixtures without fly ash addition; (a) UCS ($q_{u(28)}$)(b) three-point flexural strength (f_{dmc}), (c) segregation, (d) swelling.

In Figure 10 (a-d), 3D regression graphs demonstrate the effect of factors (F_C and F_L) on the dependent parameters for the samples produced with fly ash addition. The optimal factor values for both samples with and without fly ash addition were

determined to be F_C=%0.4 and F_L=12mm based on the dependent variables considered (as shown in Table 5). The dependent variables and desirability values corresponding to these factors are also presented in Table 5. The values of F_C=%0.4 and F_L=12mm are obtained as the optimum solution sets. In response to the F_C and F_L variation, the results of the UCS ($q_{u(28)}$), three-point flexural strength (f_{dmc}), swelling, and segregation presented in Table 5 are in good agreement with the experimental data shown in Figure 7.

The fluidity of the optimum mixtures in this research was investigated by conducting workability and setting time experiments after the optimization results were obtained. Table 5 summarizes these results. According to Szymkiewicz et al. (2013), the optimum water content of DCM material depends on the liquid limit, plasticity index, and workability limit. As shown by Szymkiewicz et al. (2013), the following equation can be used to determine the optimum water content.

$$Optimumw/LL = 0.0464(PI) + 0.5621 \quad (4)$$

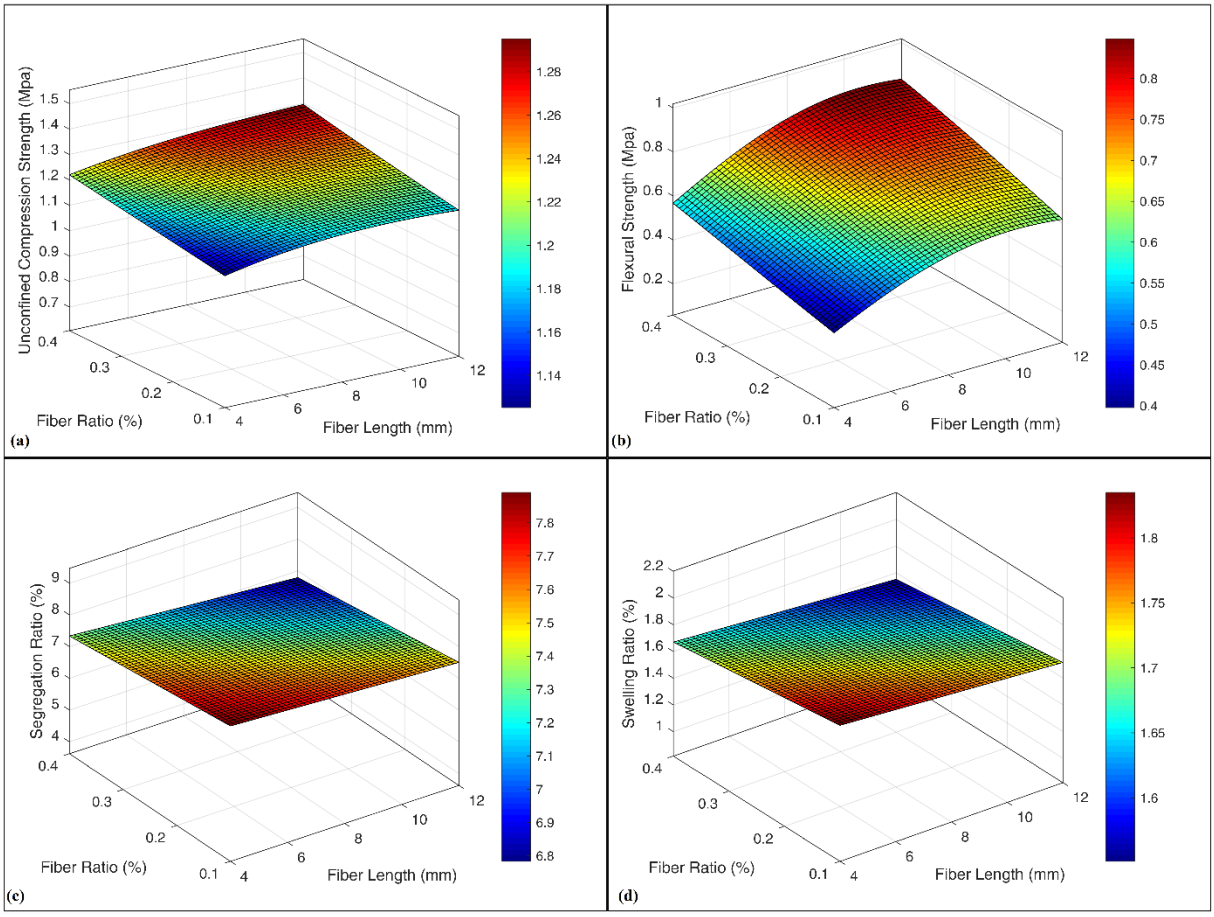

Figure 10. 3D regression plots showing the effect of factors (F_C and F_L) on the responses from the mixtures with fly ash addition; (a) UCS ($q_{u(28)}^{FA}$), (b) three-point flexural strength (f_{dmc}^{FA}), (c) segregation, (d) swelling.

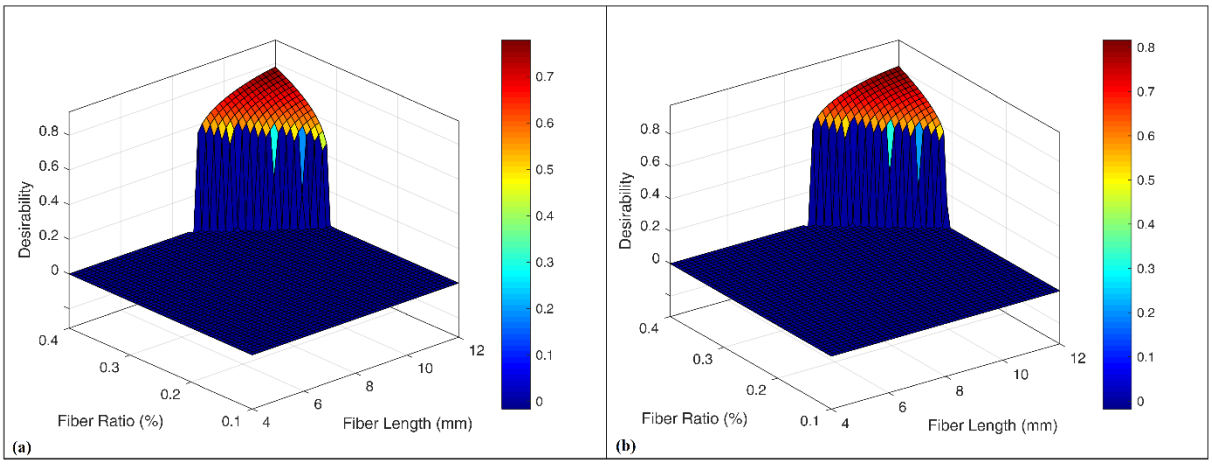

Figure 11. Composite desirability graphs obtained from optimization analyses depending on factors; (a) the mixtures without fly ash incorporation (b) the mixtures with fly ash incorporation.

As a result, Table 5 shows the values for the plastic limit, liquid limit, and plasticity index of the optimum mixtures. Values for theoretic water content were established by considering the plasticity index and liquid limit values provided in Equation 4 and Table 5. Comparing the water content of fiber-reinforced optimal mixtures to the calculated theoretical water content showed that the addition of fly ash to fiber reinforcement enhances workability. All optimum mixtures were found to be appropriate for workability.

Vicat test was performed according to ASTM C191-04b to determine the setting time of the optimum mixtures. The values for the initial and final setting times obtained for the optimum fiber-reinforced mixes are shown in Table 5 and agree well with the results obtained by Güllü et al. (2017). The results indicate that the fly ash addition with fiber incorporation increases the initial-final setting time values. Table 6 presents the statistical data of the regression graphs drawn in Figures 9 and 10, respectively. These values show that the graphs are drawn with significant statistical data.

Table 6. The statistical data of the regression graphs drawn in Figures 9 and 10, respectively.

Addition	Parameter	Unconfined compression strength	Flexural strength	Segregation ratio	Swelling ratio
Without fly ash	R^2	0.94	0.88	0.96	0.96
	RMSE	0.030	0.0550	0.124	0.0305
With fly ash	R^2	0.91	0.88	0.96	0.97
	RMSE	0.0412	0.0565	0.1233	0.0271

4. Discussion

DCM columns are frequently subjected to lateral loads in such cases of their implementations in embankments and slopes or in earthquake zones. Sukontasukkul and Jamsawang (2012) stated that various problems might be encountered if the DCM columns with insufficient flexural strength are subjected to bending moments caused by lateral loading. Some studies (Gao et al. 2017; Chen et al. 2018) emphasize that using carbon fiber effectively improves UCS and flexural strength values for the cement-soil mixes. In this presented study, along with the research of these parameters, the effects of mixture quality characteristics on the performance of DCM column materials are also examined and compared with the previous studies in the literature (e.g., Duan and Zhang 2019; Tran et al. 2018; Chen 2016; Danso et al. 2015; Zhang et al. 2015; Sharma et al. 2015; Olgun 2013). The presented research reveals that the fiber content (F_C) is the most effective factor of this study, which is demonstrated in Figure 7, and it is also confirmed by Table 3, where the contribution of factors on dependent variables is given as a percentage. The presented research also reveals that the fiber and fly ash incorporations improve the mixture quality parameters as well as the strength parameters, and this outcome agrees well with the conclusion drawn by Mohammadinia et

al. (2019). According to Chen et al. (2018), the addition of carbon fiber improves the cement composite's compressive strength by about 24% and its tensile strength in bending by 138-44%. In the presented study, the carbon fiber incorporation with soil-cement mixtures with and without fly ash addition improves the UCS results by 50-54% and the three-point flexural strength by 267-278%. As the optimum mixing ratios were determined by maximizing the three-point flexural strength in the optimization study conducted within the scope of this study, a greater improvement was achieved in the three-point flexural strength compared to the study performed by Chen et al. (2018). The presented study also specifies that the segregation and swelling ratios are improved by about 35%. This implies that the incorporation of carbon fiber can also improve the mixture quality parameters effectively.

The results of this study's multi-objective optimization analysis based on GAM are shown in Table 5. Ekmen (2020) has coupled the GAM approach with the desirability principle utilized in RSM by considering the combined desirability value and the incorporation of targets. This approach allows the optimization problem to be solved by considering the user-defined model describing the experimental values. One of the drawbacks of RSM, where the polynomial model is utilized, this drawback is eliminated by this flexibility in the novel GAM approach. Some systems with large curvature may be incompatible with the utilization of a polynomial model in RSM, as stated previously (e.g., Aydar 2018). The flexibility provided by the novel GAM approach was used to perform optimization analyses in this study, as developed in the study of Ekmen (2020).

5. Conclusions and comments

Based on the investigations, the following conclusions can be drawn.

1. The inclusion of carbon fiber in the mixture results in a noteworthy improvement in the mixture quality parameters, such as segregation and swelling ratios, by up to 35%. Furthermore, it has increased the unconfined compressive strength by 54% and the three-point flexural strength by up to 278%.
2. The fiber content is identified to be the most significant factor compared to the fiber length.
3. The three-point flexural strength (f_{dmc}) is affected by fiber content and length variations. Optimum UCS ($q_{u(28)}$), three-point flexural strength (f_{dmc}), segregation and swelling percentage are specified as approximately 1.3 MPa, 0.8 MPa, 6.73%, and 1.57% for samples without fly ash admixture, respectively. The values of 1.3 MPa, 0.83 MPa, 6.78%, and 1.55% were identified for the mixtures with fly ash addition.
4. The optimum factors are specified as 0.4% for fiber content and 12 mm for fiber length.
5. A balanced optimization solution was presented with GAM by minimizing the factors that increase the cost to provide the needed improvement. As a result of the workability and setting time tests conducted to measure the applicability of the optimum mixtures, it was determined that all the optimum mixtures were appropriate.
6. The optimization solution incorporating fly ash has shown a higher level of desirability, as per the research findings.
7. The inclusion of fly ash in the optimal mixture for DCM column production results in improved setting time and workability, making it a more suitable option than the mixture without fly ash.
8. The desirability concept in RSM was incorporated into the optimization algorithm of GAM, which was developed and used in this study. It is demonstrated that it is an efficient analysis approach using nonlinear programming, which highlights the significance of introducing the user-defined high-level models to the presented experimental data that can enhance the performance of optimization solutions.

Author contributions: ABE; Data processing, experimental study, writing. HMA; Conceptualization, writing, revising.

Funding: The Scientific Research Projects Coordination Unit of Harran University, Turkiye, funded this study (HUBAP project no: 18253).

Conflicts of interest: The authors declare no conflict of interest.

References

Algin, H.M. (2016). Optimised design of jet-grouted raft using response surface method. Computers and Geotechnics, 74, 56-73. https://doi.org/10.1016/j.compgeo.2015.12.012

Algin, H.M. (2018). Optimised design of jet-grouted rafts subjected to nonuniform vertical loading. KSCE J Civ Eng 22, 494–508. https://doi.org/10.1007/s12205-017-0841-1

Anggraini, V., Asadi, A., Syamsir, A., & Huat, B. B. (2017). Three point bending flexural strength of cement treated tropical marine soil reinforced by lime treated natural fiber. Measurement, 111, 158-166. https://doi.org/10.1016/j.measurement.2017.07.045

ASTM C1609 / C1609M-19. (2019) Standard Test Method for Flexural Performance of Fiber-Reinforced Concrete (Using Beam With Third-Point Loading), ASTM International, West Conshohocken, PA. https://doi.org/10.1520/C1609_C1609M-19

ASTM C1610 / C1610M-17. (2017) Standard Test Method for Static Segregation of Self-Consolidating Concrete Using Column Technique, ASTM International, West Conshohocken, PA. https://doi.org/10.1520/C1610_C1610M-17

ASTM D4546-14, Standard Test Methods for One-Dimensional Swell or Collapse of Soils, ASTM International, West Conshohocken, PA, 2014 https://doi.org/10.1520/D4546-14

ASTM C191-04b. (2004). Standard Test Method for Time of Setting of Hydraulic Cement by Vicat Needle, ASTM International, West Conshohocken, PA. https://doi.org/10.1520/C0191-04B

ASTM D2166 / D2166M-16. (2016). Standard Test Method for UCS of Cohesive Soil, ASTM International, West Conshohocken, PA. https://doi.org/10.1520/D2166_D2166M-16

ASTM D 4767-88. (1993). Standard test method for consolidated-undrained triaxial compression test on cohesive soils. Annual book of ASTM standards, Philadelphia, PA, 04.08, 1071-1081.

Avci, Y., & Ekmen, A. B. (2023, October). Artificial intelligence assisted optimization of rammed aggregate pier supported raft foundation systems based on parametric three-dimensional finite element analysis. In Structures (Vol. 56, p. 105031). Elsevier.

Aydar, A. Y. (2018). Utilization of response surface methodology in optimization of extraction of plant materials. Statistical Approaches With Emphasis on Design of Experiments Applied to Chemical Processes. InTech, 157-169. https://doi.org/10.5772/intechopen.73690

Ben-Gal, I. (2005). On the use of data compression measures to analyze robust designs. IEEE Transactions on Reliability, 54(3), 381-388. https://doi.org/10.1109/TR.2005.853280

Bergado, D. T., Ruenkrairergsa, T., Taesiri, Y., & Balasubramaniam, A. S. (1999). Deep soil mixing used to reduce embankment settlement. Proceedings of the Institution of Civil Engineers-Ground Improvement, 3(4), 145-162. https://doi.org/10.1680/gi.1999.030402

Boehm, D. W. (2004). The utilization of jet grouting and soil mixing methods to repair and support bulkhead structures. In Ports 2004: Port Development in the Changing World (pp. 1-10). https://doi.org/10.1061/40727(2004)96

Broms, B. B. (1986). Stabilization of soft clay with lime and cement columns in Southeast Asia. Applied Research Project RP10/83, Nanyang Technological Institute, Singapore. https://hdl.handle.net/10356/46576

Bruce, M. E. C., Berg, R. R., Collin, J. G., Filz, G. M., Terashi, M., Yang, D. S., & Geotechnica, S. (2013). Federal Highway Administration design manual: Deep mixing for embankment and foundation support (No. FHWA-HRT-13-046). United States. Federal Highway Administation. Offices of Research & Development.

Chen, J., Lee, F. H., & Ng, C. C. (2011). Statistical analysis for strength variation of deep mixing columns in Singapore. In Geo-Frontiers 2011: Advances in Geotechnical Engineering (pp. 576-584). https://doi.org/10.1061/41165(397)60

Chen, Z. S., Zhou, X., Wang, X., & Guo, P. (2018). Mechanical behavior of multilayer GO carbon-fiber cement composites. Construction and Building Materials, 159, 205-212.https://doi.org/10.1016/j.conbuildmat.2017.10.094

Chen, F. (2016). Experiment research on tensile strength of basalt fiber cement-soil. Journal of Shenzhen University Science and Engineering, 33(2), 188-193.

Croce, P., Flora, A., & Modoni, G. (2014). Jet grouting: technology, design and control. CRC Press.

Danso, H., Martinson, D. B., Ali, M., & Williams, J. B. (2015). Physical, mechanical and durability properties of soil building blocks reinforced with natural fibres. Construction and Building Materials, 101, 797-809. https://doi.org/10.1016/j.conbuildmat.2015.10.069

Dehghanbanadaki, A., Rashid, A. S. A., Ahmad, K., Yunus, N. Z. M., & Motamedi, S. (2023). Deep soil mixing stabilisation of peat: a review of small-scale and 1 g physical modelling test results. Bulletin of Engineering Geology and the Environment, 82(5), 1-15.

Duan, X. L., & Zhang, J. S. (2019). Mechanical properties, failure mode, and microstructure of soil-cement modified with fly ash and polypropylene fiber. Advances in Materials Science and Engineering, 2019. https://doi.org/10.1155/2019/9561794

Ekmen, A. B. (2020). Three-dimensional lithological modelling of soils using field test results and utilisation of the developed method in numerical analysis of deep mixing columns. Ph. D. Thesis, Harran University, Civil Engineering Department, Turkey.

Ekmen, A. B., Algin, H. M., & Özen, M. (2020). Strength and stiffness optimisation of fly ash-admixed DCM columns constructed in clayey silty sand. Transportation Geotechnics, 24, 100364.

Ekmen, A. B. (2023). Evaluation of SPT-N values and internal friction angle correlation using artificial intelligence methods in granular soils. Soil Research.

Ekmen, A. B., & Avci, Y. (2023). Artificial Intelligence-Assisted Optimization of Tunnel Support Systems Based on the Multiple Three-Dimensional Finite Element Analyses Considering the Excavation Stages. Iranian Journal of Science and Technology, Transactions of Civil Engineering, 47(3), 1725-1747.

Elkhebu, A., Zainorabidin, A., Asadi, A., Bakar, I. H., Huat, B. B., Abdeldjouad, L., & Dheyab, W. (2020). Effect of incorporating multifilament polypropylene fibers into alkaline activated fly ash soil mixtures. Soils and Foundations. https://doi.org/10.1016/j.sandf.2019.11.015

Flora, A., Modoni, G., Lirer, S., & Croce, P. (2013). The diameter of single, double and triple fluid jet grouting columns: prediction method and field trial results. Géotechnique, 63(11), 934-945. https://doi.org/10.1680/geot.12.P.062

Gao, L., Zhou, Q., Yu, X., Wu, K., & Mahfouz, A. H. (2017). Experimental study on the UCS of carbon fiber reinforced clay soil. Marine Georesources & Geotechnology, 35(1), 143-148. https://doi.org/10.1080/1064119X.2015.1102184

Gembicki, F. W. (1974). Vector optimization for control with performance and parameter sensitivity indices. Ph. D. thesis, Case Western Reserve Univ.

Golder Associates. (2013). High level geotechnical input: Fishermans Bend development. Rep. No. 127613038-003-R. Decatur, AL: Golder Associates.

Güllü, H., Canakci, H., & Al Zangana, I. F. (2017). Use of cement based grout with glass powder for deep mixing. Construction and Building Materials, 137, 12-20. https://doi.org/10.1016/j.conbuildmat.2017.01.070

Kafodya, I., & Okonta, F. (2018). Effects of natural fiber inclusions and pre-compression on the strength properties of lime-fly ash stabilised soil. Construction and Building Materials, 170, 737-746. https://doi.org/10.1016/j.conbuildmat.2018.02.194

Kamon, M. (1996, May). Effects of Grouting and DMM on Big Construction Projects In Japan and the 1995 Hyogoken-Nambu Earth Quake. In Proc. 2nd International Conference on Ground Improvement Geosystems, Tokyo,(2) (pp. 807-823).

Lai, Y. P., Bergado, D. T., Lorenzo, G. A., & Duangchan, T. (2006). Full-scale reinforced embankment on deep jet mixing improved ground. Proceedings of the Institution of Civil Engineers-Ground Improvement, 10(4), 153-164. https://doi.org/10.1680/grim.2006.10.4.153

Liu, G. P., Yang, J. B., & Whidborne, J. F. (2003). Multiobjective optimisation and control. Research Studies Press.

Liu, Y., He, L. Q., Jiang, Y. J., Sun, M. M., Chen, E. J., & Lee, F. H. (2019). Effect of in situ water content variation on the spatial variation of strength of deep cement-mixed clay. Géotechnique, 69(5), 391-405. https://doi.org/10.1680/jgeot.17.P.149

Liu, Y., Lee, F. H., Quek, S. T., Chen, E. J., & Yi, J. T. (2015). Effect of spatial variation of strength and modulus on the lateral compression response of cement-admixed clay slab. Géotechnique, 65(10), 851-865. https://doi.org/10.1680/jgeot.14.P.254

Lorenzo, G. A., & Bergado, D. T. (2004). Fundamental parameters of cement-admixed clay—New approach. Journal of geotechnical and geoenvironmental engineering, 130(10), 1042-1050. https://doi.org/10.1061/(ASCE)1090-0241(2004)130:10(1042)

Lorenzo, G. A., & Bergado, D. T. (2006). Fundamental characteristics of cement-admixed clay in deep mixing. Journal of materials in civil engineering, 18(2), 161-174. https://doi.org/10.1061/(ASCE)0899-1561(2006)18:2(161)

Matlab, (2017). Matlab, version R2017a, MathWorks.

Miura, N., Horpibulsuk, S., & Nagaraj, T. S. (2001). Engineering behavior of cement stabilized clay at high water content. Soils and Foundations, 41(5), 33-45. https://doi.org/10.3208/sandf.41.5_33

Mohammadinia, A., Disfani, M. M., Conomy, D., Arulrajah, A., Horpibulsuk, S., & Darmawan, S. (2019). Utilization of Alkali-Activated Fly Ash for Construction of Deep Mixed Columns in Loose Sands. Journal of Materials in Civil Engineering, 31(10), 04019233. https://doi.org/10.1061/(ASCE)MT.1943-5533.0002878

Mohammadinia, A., Arulrajah, A., Horpibulsuk, S., & Shourijeh, P. T. (2019). Impact of potassium cations on the light chemical stabilization of construction and demolition wastes. Construction and Building Materials, 203, 69-74. https://doi.org/10.1016/j.conbuildmat.2019.01.083

Mohammadinia, A., Arulrajah, A., D'Amico, A., & Horpibulsuk, S. (2018). Alkali-activation of fly ash and cement kiln dust mixtures for stabilization of demolition aggregates. Construction and Building Materials, 186, 71-78. https://doi.org/10.1016/j.conbuildmat.2018.07.103

Myers RH, Montgomery DC, Anderson-Cook CM. (2009). Response Surface Methodology: Process and Product Optimization Using Designed Experiments: Wiley.

Olgun, M. (2013). Effects of polypropylene fiber inclusion on the strength and volume change characteristics of cement-fly ash stabilized clay soil. Geosynthetics International, 20(4), 263-275. https://doi.org/10.1680/gein.13.00016

Porbaha, A. (1998). State of the art in deep mixing technology: part I. Basic concepts and overview. Proceedings of the Institution of Civil Engineers-Ground Improvement, 2(2), 81-92. https://doi.org/10.1680/gi.1998.020204

Porbaha, A., Shibuya, S., & Kishida, T. (2000). State of the art in deep mixing technology. Part III: geomaterial characterization. Proceedings of the Institution of Civil Engineers-Ground Improvement, 4(3), 91-110. https://doi.org/10.1680/grim.2000.4.3.91

Pradeep G. (2008). Response surface method. Saarbrücken, Germany: VDM Verlag Publishing.

Ramadas, T. L., Kumar, N. D., & Aparna, G. (2010, December). Swelling and strength characteristics of expansive soil treated with stone dust and fly Ash. In Indian geotechnical conference (pp. 557-560).

Shahin, M. A., & Cargeeg, A. (2011). Experimental Investigation into Multistage versus Conventional Triaxial Compression Tests for a c-phi Soil. In Applied Mechanics and Materials (Vol. 90, pp. 28-32). Trans Tech Publications Ltd. https://doi.org/10.4028/www.scientific.net/AMM.90-93.28

Sharma, V., Vinayak, H. K., & Marwaha, B. M. (2015). Enhancing compressive strength of soil using natural fibers. Construction and Building Materials, 93, 943-949. https://doi.org/10.1016/j.conbuildmat.2015.05.065

Shen, S. L., Wang, Z. F., Yang, J., & Ho, C. E. (2013). Generalized approach for prediction of jet grout column diameter. Journal of Geotechnical and Geoenvironmental Engineering, 139(12), 2060-2069. https://doi.org/10.1061/(ASCE)GT.1943-5606.0000932

Soranzo, M. (1988). Results and interpretation of multistage triaxial compression tests. In Advanced triaxial testing of soil and rock. ASTM International.

Sukontasukkul, P., & Jamsawang, P. (2012). Use of steel and polypropylene fibers to improve flexural performance of deep soil–cement column. Construction and Building Materials, 29, 201-205. https://doi.org/10.1016/j.conbuildmat.2011.10.040

Szymkiewicz, F., Tamga, F. S., Kouby, A. L., & Reiffsteck, P. (2013). Optimization of strength and homogeneity of deep mixing material by the determination of workability limit and optimum water content. Canadian geotechnical journal, 50(10), 1034-1043. https://doi.org/10.1139/cgj-2012-0327

Terashi, M. (2005). Keynote lecture: design of deep mixing in infrastructure applications. In Proc. Int'l Conf on Deep Mixing-Best Practice and Recent Advances, 2005.

Tran, K. Q., Satomi, T., & Takahashi, H. (2018). Improvement of mechanical behavior of cemented soil reinforced with waste cornsilk fibers. Construction and Building Materials, 178, 204-210. https://doi.org/10.1016/j.conbuildmat.2018.05.104

Wang, D., Wang, H., Larsson, S., Benzerzour, M., Maherzi, W., & Amar, M. (2020). Effect of basalt fiber inclusion on the mechanical properties and microstructure of cement-solidified kaolinite. Construction and Building Materials, 241, 118085. https://doi.org/10.1016/j.conbuildmat.2020.118085

Wang, D., Tawk, M., Indraratna, B., Heitor, A., & Rujikiatkamjorn, C. (2019). A mixture of coal wash and fly ash as a pavement substructure material. Transportation Geotechnics, 21, 100265. https://doi.org/10.1016/j.trgeo.2019.100265

Watabe, Y., Tsuchida, T., Furuno, T., & Yuasa, H. (2000). Mechanical characteristics of a cement treated dredged soil utilized for waste reclamation landfill. Coastal geotechnical engineering in practice, A. Nakasa and T. Tsuchida, eds., Balkema, Rotterdam, Netherlands, 739-745.

Wu, M., Zhao, X., & Dou, Y. M. (2005). Application of stiffened deep cement mixed column in ground improvement. In Proceedings international conference on deep mixing best practices and recent advances, Stockholm, Sweden (pp. 463-468).

Yin, J. H. (2001). Stress-strain-strength characteristics of soft Hong Kong marine deposits without or with cement treatment. Lowland Technology International, 3(1, June), 1-13.